XL CILAMCE
IBERO-LATIN AMERICAN CONGRESS ON COMPUTATIONAL METHODS IN ENGINEERING
NOVEMBER 11-14, 2019
Praiamar Natal Hotel & Convention
Natal, RN-BRAZIL

NUMERICAL MODELLING OF AXIAL HYDROCYCLONE – PHASE SEGREGATION OF DISPERSED OIL IN CONTINUOUS WATER PHASE

Rodrigo V. Cabral
André D. Rocha
rodrigo.cabral@ufabc.edu.br
a.damiani@ufabc.edu.br
Energy Engineering Modeling and Simulation Laboratory (EEMSL) - Federal University of ABC
Av. dos Estados 5001 - Bangú, 09210-580, Santo André/SP, Brazil

Abstract. This paper presents a numerical model of the particle trajectory in an axial hydrocyclone under laminar flow conditions using Discrete Phase Model (DPM). The DPM is an implementation of Lagrangian particle tracking which is essentially a means of tracking discrete particles through a continuum of fluid. The primary phase (continuous phase) is water and the second phase (discrete phase) is oil. The numerical analysis has been carried for laminar axial Reynolds numbers along a 91.2 mm internal diameter size and 2.7 m long pipe. The swirling flow is generated from static swirler with 7 vanes, deflection angle of 65.5°, and a gap width of 5 mm. The particle trajectory was obtained for two Reynolds numbers (150 and 300) and three different diameters (10, 100 e 1000 μm). From this conditions it is possible to conclued that the larger particle diameter the closer to the center of thecan get closer to the center of the tube along the dowstream flow of the swirler. Besides that, the Reynolds number impact shows that how smaller it was, the closer to the center the particle remais and reaches a stable radial position.

Keywords: hydrocyclone, axial inlet, particle trajectory, computational fluid dynamics.

1 Introduction

Liquid-liquid separation hydrocyclones are widely used in various industries for the removal of water-dispersed oil, especially for final water purification processes, where the oil concentration is below 1% of the continuous water phase. With this thorough application, hydrocyclones become important for example in the application of oilfields where platforms require small size devices and high separation efficiency due to stringent environmental laws for discharging oil extraction waters rough from the bottom of the sea. In general, hydrocyclones are separated into two distinct classes, those of tangential input as studied by Narasimha et al. [1], and axial input hydrocyclones as studied by Rocha et al. [2] . Although they are distinguished in classification, they have the same principle of operation, where the objective is to separate two phases of close density by applying a centrifugal flow to the flow, inducing separation by density difference, where the lower density fluid tends to go to the center and the highest density to the periphery of the flow. One of the first studies on laminar swirl flow was performed by Talbot [3], using an analytical and experimental approach to low Reynolds numbers. Dirkzwager [4] was one of the first to design an axial inlet liquid-liquid separator. Subsequently, several authors compared numerical and experimental results observing their quantitative differences and physical separation principles, even for a monophasic and laminar flow, as it was the case of Rocha et al. [2] and Rocha et al. [5]. The numerical and experimental study Slot et al. [6] was performed for an axial hydrocyclone flow aiming at the oil-water separation, aiming at a better observation of the oil extraction point a continuous phase of water, ranging in size from 50 to 200 micrometers. The objective of this work is to investigate the behavior of an oil particle immersed in a continuous aqueous phase after applying a fixed vane-induced centrifugal field to a laminar flow, applying the Discrete Phase Model theory with the tool $Ansys^{®}Fluent$. This research aims to analyze the flow behavior against a different geometry from literature.There are differences in the geometry herein on blade shape and on the deflection angle.For this, the flow conditions will vary with Reynolds number, between 150 and 300, and with particle diameter, between 10 μm and 1000 μm.

2 Swirler

The geometry used in the present study was designed by Cabral and Rocha [7] and is based on the work of Rocha et al. [2]. The swirler has been designed based on a deflection angle of $63.5°$ and consists in a spherical nose leading edge, an annulus section with 7 vanes and conical trailing edge, as shown in Fig. 1.

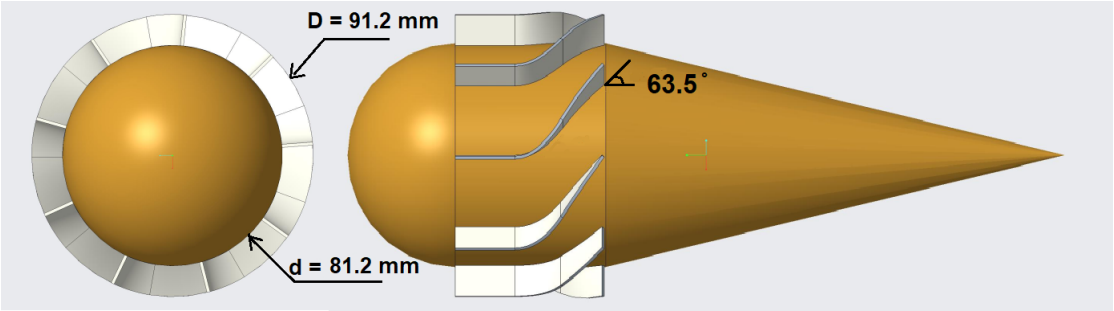

Figure 1. Swirler representation

3 Modeling

The flow modeling was separated into two parts. First, the governing equations were used for a monophasic flow through the Eulerian methodology. The results of tangential velocity, axial velocity

and pressure drop were used in the independence study. Then, the discrete phase modeling that considers an oil particle in the folding is performed using the Lagrangian methodology.

3.1 Numerical modeling

The flow as a whole was modeled from the fundamental principles of classical fluid mechanics, expressing the conservation of mass and momentum. The flow is assumed as laminar, isothermal regime with constant, incompressible and three-dimensional properties. Gravitational effects were neglected. Thus the reduced set of equations in cylindrical coordinates (θ, r, z) with (u, v, w) the velocity components are described below:

Equation of continuity

$$\frac{1}{r}\frac{\partial(rv)}{\partial r} + \frac{1}{r}\frac{\partial(u)}{\partial \theta} + \frac{\partial w}{\partial z} = 0 \tag{1}$$

Momentum – radial direction (r)

$$\rho\left(v\frac{\partial v}{\partial r} + \frac{u}{r}\frac{\partial v}{\partial \theta} - \frac{u^2}{r} + w\frac{\partial v}{\partial z}\right) = -\frac{\partial p}{\partial r} + \mu\left\{\frac{\partial}{\partial r}\left[\frac{1}{r}\frac{\partial}{\partial r}(rv)\right] + \frac{1}{r^2}\frac{\partial^2 v}{\partial \theta^2} - \frac{2}{r^2}\frac{\partial u}{\partial \theta} + \frac{\partial^2 v}{\partial w^2}\right\} \tag{2}$$

Momentum – tangential or circumferential direction (θ)

$$\rho\left(v\frac{\partial u}{\partial r} + \frac{u}{r}\frac{\partial u}{\partial \theta} + \frac{vu}{r} + w\frac{\partial u}{\partial z}\right) = -\frac{1}{r}\frac{\partial p}{\partial \theta} + \mu\left\{\frac{\partial}{\partial r}\left[\frac{1}{r}\frac{\partial}{\partial r}(ru)\right] + \frac{1}{r^2}\frac{\partial^2 u}{\partial \theta^2} + \frac{2}{r^2}\frac{\partial v}{\partial \theta} + \frac{\partial^2 u}{\partial w^2}\right\} \tag{3}$$

Momentum – axial direction (z)

$$\rho\left(v\frac{\partial w}{\partial r} + \frac{u}{r}\frac{\partial w}{\partial \theta} + w\frac{\partial w}{\partial z}\right) = -\frac{\partial p}{\partial z} + \mu\left\{\frac{1}{r}\frac{\partial}{\partial r}\left(r\frac{\partial w}{\partial r}\right) + \frac{1}{r^2}\frac{\partial^2 w}{\partial \theta^2} + \frac{\partial^2 w}{\partial z^2}\right\} \tag{4}$$

Fluid density and dynamic viscosity properties are represented by ρ and μ, respectively.

3.2 Computational modeling

The Eqs. (1), (2), (3) and (4) using the Finite Volume Method using the $Ansys^{®}Fluent$ code. For the solver, the pressure-based Coupled function was used, where it solves pressure and momentum simultaneously. This algorithm is applicable for most single-phase flows and produces superior performance for cyclonic separators Fluent [8]. For the discretization system, second order upwind was used for pressure and momentum equations to ensure good accuracy. The computational convergence criteria are guaranteed when the residuals are less than 10^{-6}. The flow domain is shown in Fig. 2.

The boundary conditions must be specified to solve the governing equations. On input, the average velocity is specified and is calculated as a function of the Reynolds number, as Eq. (5).

$$Re = \frac{\rho v D}{\mu} \tag{5}$$

where ρ is density of fluid, v the average velocity at the inlet, D the pipe diameter and μ the dynamic viscosity. Table 1 presents

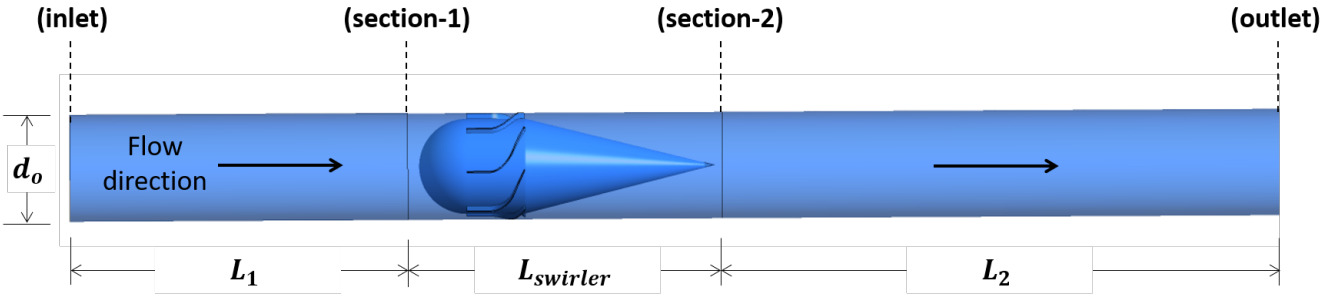

Figure 2. Computational domain

Table 1. Dimensions of computational domain, testing conditions and fluid properties.

Parameter	Quantity
1. Tube length (m)	2.77
2. Inner diameter (mm)	91.2
3. Deflection angle	63.5°
4. Working fluid	Water
5. Density @ 25°C (kg/m3)	998.2
6. Viscosity @ 25°C (Pa.s)	0.001
7. Reynolds number	150 and 300

At the output, there is no information about the variables studied and some assumptions must be made, the diffusion flows in the normal direction to the output plane are assumed to be zero, the pressure at the outlet section is specified. The pipe walls adopt the non-slip condition.

Mesh generation is a key step in achieving good simulation accuracy. In this study, a tetrahedral mesh was generated from the $Ansys^{®}Meshing$ software. Fig. 3 shows the final mesh used.

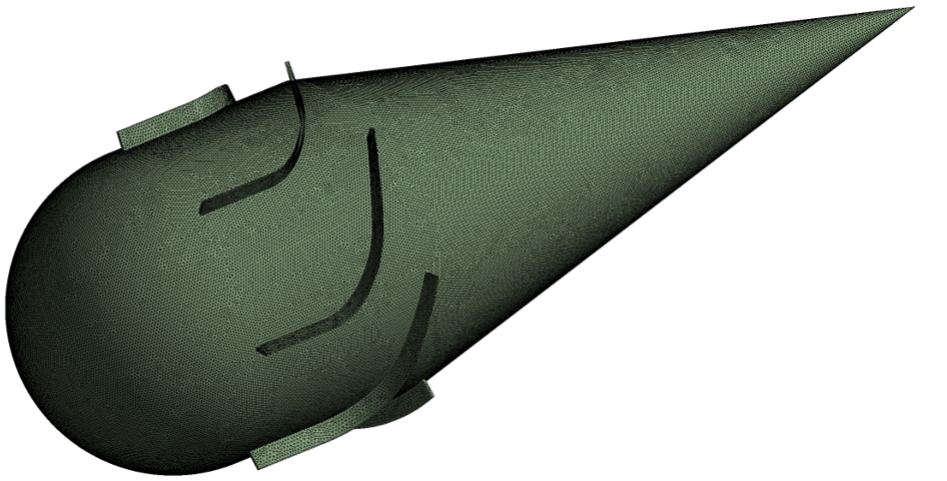

Figure 3. Mesh of swirler

To ensure the accuracy of the mesh used, the Grid Convergence Index (GCI) mesh independence method developed by Roache [9] was applied. Three meshes were used to apply the generalized Richardson extrapolation, reporting discretization errors. Three distinct meshes and three variables (tangential velocity, axial velocity and pressure drop) downstream of the swirler were used to verify the indepen-

dence of the results according to the refinement of each mesh. Table 2 shows the GCI results.

Table 2. Grid Convergence Index for Re = 50. M1, M2 and M3 are the coarse to the fine meshes. CN = cells number.
RF = refinement factor. Extr. = Richardson Extrapolation.

Mesh	**CN**	**RF**	$W_{blade-out}$	GCI	$U_{blade-out}$	GCI	$\Delta p_{swirler}$	GCI
-	-	-	[m/s]	[%]	[m/s]	[%]	[Pa]	[%]
M1	1,990,651	-	0.002733	-	0.002560	-	0.198016	-
M2	5,172,417	1.37	0.002786	-	0.002641	-	0.204600	-
M3	15,409,880	1.44	0.002820	1.62	0.002682	1.37	0.207773	1,24
Extr.	-	-	**0.002857**	-	**0.002712**	-	**0.209800**	-

The average tangential and axial velocities in the downstream section of the swirler for mesh validation are calculated from Eq. (6).

$$\bar{V} = \frac{\int_A V dA}{\int_A dA} \tag{6}$$

The pressure drop, the third variable used to validate the mesh, is defined as a mean pressure difference at the swirler inlet section (section 1) and the mean outlet pressure (section 2) as:

$$p = \bar{p_1} - \bar{p_2} \tag{7}$$

where the mean pressure is defined as:

$$\bar{p} = \frac{\int_A p dA}{\int_A dA} \tag{8}$$

3.3 Discrete Phase Model

For the computational modeling of multiphase flow one of the approaches used is the Euler-Lagrange. This model treats the fluid phase as a continuum by solving the continuity and Navier-Stokes equations, while The dispersed phase is solved by tracing particles, bubbles or droplets across the calculated flow field. This approach is considerably simpler when particle interactions can be neglected, this requires that the dispersed phase occupies a low volume fraction, which is the case with this work. Another simplification adopted for this model disregards the influence of the particle in the flow as a whole, only the continuous phase changes the particles trajectory. To calculate the trajectory traveled, a force balance is applied from Newton's second law:

$$\frac{dv_p}{dt} = F_D(\vec{u} - \vec{u}_p) + \frac{\vec{g}(\rho_p - \rho)}{\rho_p} + \vec{F} + \vec{G} \tag{9}$$

where $\vec{F}$ is an additional acceleration term.

Since the particle Reynolds numbers is insure below the unit value, the drag force term can be calculated as follows:

$$F_D = \frac{18\mu}{\rho_p dp^2} \frac{C_D Re}{24} \tag{10}$$

where u is the average velocity of the continuous phase, u_p the velocity of the fluid particle, μ is the viscosity of the particle, ρ is the density of the continuous phase, ρ_p is the particle density, and d_p is the particle diameter. Re is the relative Reynolds number, defined by:

$$Re \equiv \frac{\rho d_p \left|\vec{u}_p - \vec{u}\right|}{\mu} \tag{11}$$

For additional forces, in addition to the drag force, there is the force due to the virtual mass that requires a fluid acceleration in the particle.

$$\vec{F} = \frac{1}{2}\frac{\rho}{\rho_p}\frac{d}{dt}(\vec{u} - \vec{u}_p) \tag{12}$$

The other force that must be considered is due to the pressure gradient caused by the flow, since $\rho > \rho_p$ because the ultimate goal is to direct the oil particle to the center of the pipe, so it has the following expression:

$$\vec{G} = \left(\frac{\rho}{\rho_p}\right) u_p \bigtriangledown u \tag{13}$$

The values used for DPM calculation are shown in Table 3.

Table 3. Dispersed Phase Parameters

Description	Value
1. Particle	oil
2. Particle Diameter (μm)	10, 100 and 1000
3. Particle Density (kg/m3)	$\rho = 800$
4. Particle Velocity (m/s)	$\vec{u}_p = 0.001653; \vec{u}_p = 0.003305$
5. Particle Reynolds	$0 \leq Re \leq 1$

4 Results and discussions

The trajectories were obtained numerically considering a spherical fluid particle. Only the continuous phase flow interferes with the particle's trajectory. Fig. 4 shows the trajectory of an oil particle for the Reynolds of flow of 300 and three different particle diameters. The particle is released into the inlet region of the flow. It is noted that the particle acquires a centrifugal field after passing through the hydrocyclone ring where the flow is deflected by the vanes. This field causes the smaller diameter oil fluid particle to have a larger spin in the cone region. Downstream of the generator, the fluid particle spin is dampened due to viscous effects. Drag and density are the main terms affected by fluid particle size. This effect is shown in Fig. 5. Corroborating with a drag force equation, note whether Fig. 5 that the particle diameter directly influences its trajectory, where for the smallest diameter the drag force is larger and consequently throws a particle to the pipe periphery.

The 2D trajectory of the fluid particle is shown in Fig. 5. The studied particles have lower density when compared to the continuous phase. This means that in centrifugal field the lighter particles segregate towards the center of the tube. When comparing the trajectory of particles of different diameters, note that the heaviest particle (D1) approaches the center at a distance (y) of approximately 1.65 m. The intermediate diameter particle (D2) approaches the center at a distance of 1.82 m and the lightest particle (D3) approaches the center at a distance of 2.61 m. After approximately 2.1 m the particles move away from the center. This is due to spin decay, the tangential velocity component dissipates and the centrifugal field loses its intensity.

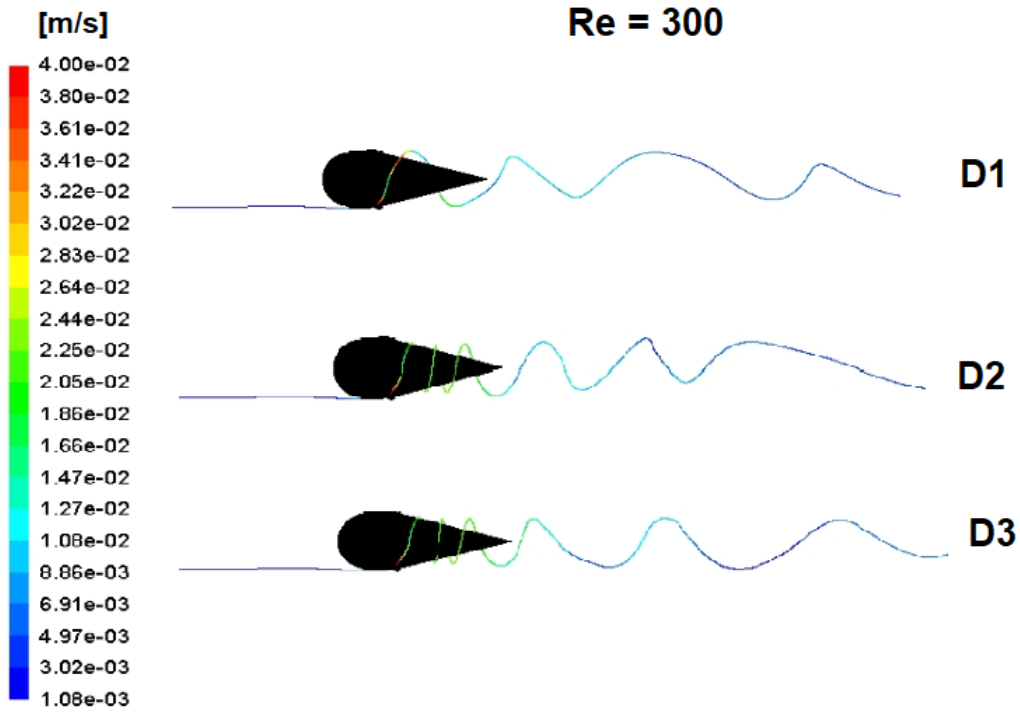

Figure 4. Magnitude velocity ($D_1 = 1000\mu m$, $D_2 = 100\mu m$, $D_3 = 10\mu m$)

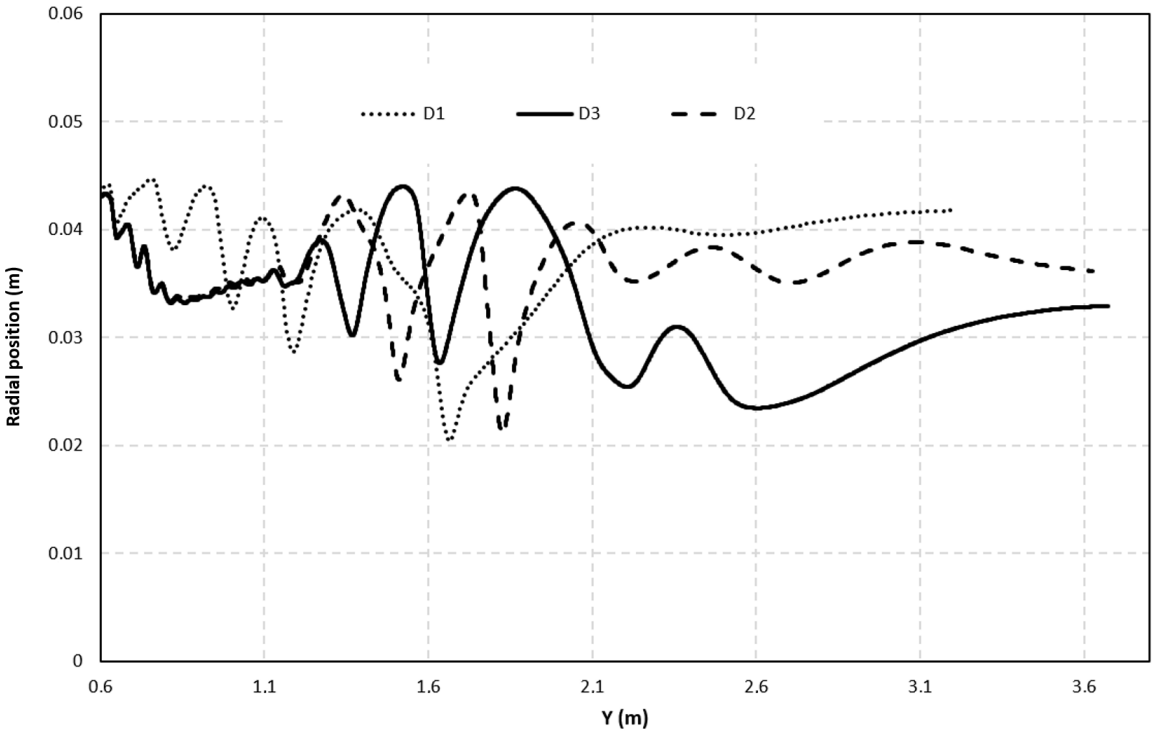

Figure 5. Variation of radial position of downstream particle flow.

The particle trajectory for different Reynolds numbers is shown in Fig. 6. By varying the continuous phase Reynolds for the same fluid particle diameter (D1) it was observed that for the smallest value (Re=150) the particle has a longer permanence and closer to the center of the pipe. This effect can be explained by The tangential velocity field strength has a lower value than the Reynolds 300. Note that this same effect can also be seen by a lower spin intensity and earlier dissipation.

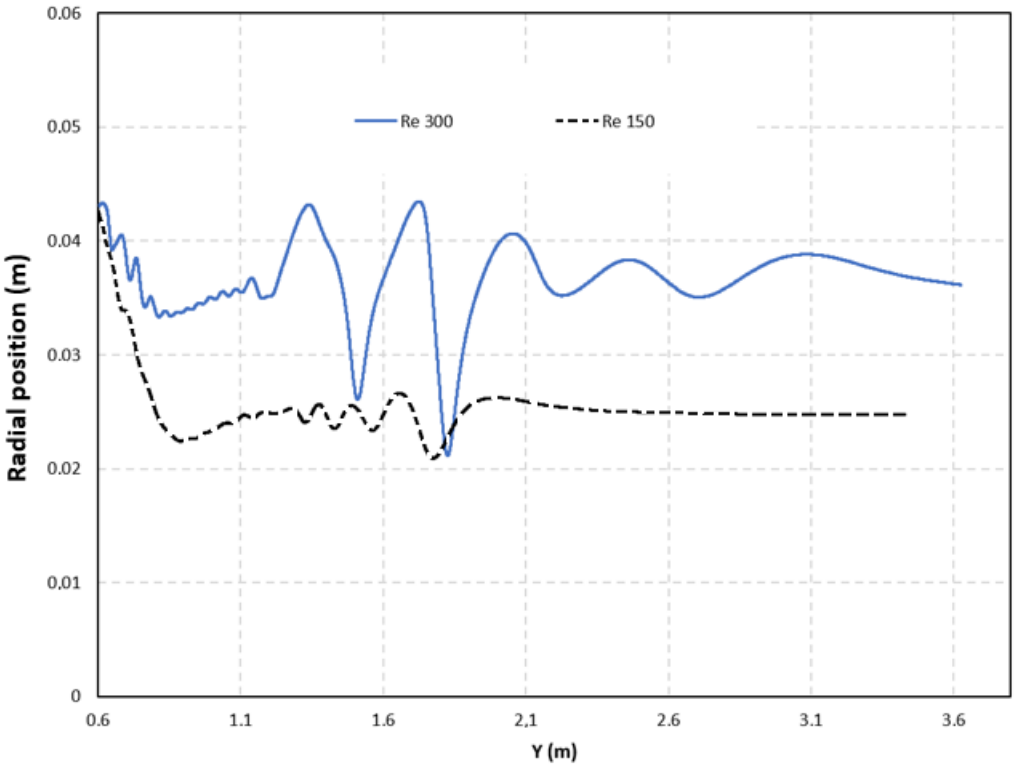

Figure 6. Variation of radial position of downstream particle flow

5 Conclusion

The project seeks to analyze the flow behavior against a different geometry from literature. There are differences in the geometry herein on blade shape and on the deflection angle. Although the adopted model has numerous simplifications, it is possible to notice the behavior of an oil particle dispersed in a continuous water phase after application of a centrifugal field through an axial inlet hydrocyclone. For the conditions imposed by this study, it was noted that the larger the particle diameter the closer to the center of the tube it approaches, along the downstream flow of the swirler. Regarding the variation of Reynolds, it was noted that due to the tangential velocity field imposed by the swirler the smaller the Reynolds the closer to the center the particle remains and reaches a stable radial position. These conditions are important because for the design of an extraction pipe, it is necessary to optimize the position where such apparatus should be installed to remove the dispersed phase of the continuous phase.

Acknowledgment

The authors would like to acknowledge CAPES (Coordination for the Improvement of Higher Education Personnel) for Grant and FAPESP (São Paulo Research Foundation) for scientific support 2017/06978-3.

References

[1] Narasimha, M., Sripriya, R., & Banerjee, P. K., 2004. Cfd modelling of hycrocyclone - prediction of cut size. *International Journal of Mineral Processing*.

[2] Rocha, A. D., Bannwart, A. C., & Ganzarolli, M. M., 2015. Numerical and experimental study of an axially induced swirling pipe flow. *International Journal of Heat and Fluid Flow*, vol. 53, pp. 81–90.

[3] Talbot, L., 1951. Study of laminar swirling pipe flow. *PhD Thesis, University of Michigan*.

[4] Dirkzwager, M., 1996. A new axial cyclone design for fluid-fluid separation. *PhD thesis, Delft University of Technology*.

[5] Rocha, A. D., Bannwart, A. C., & Ganzarolli, M. M., 2017. Effects of inlet boundary conditions in an axial hydrocyclone. *Journal of the Brazilian Society of Mechanical Sciences and Engineering*, vol. 39, n. 9, pp. 3425–3437.

[6] Slot, J. J., Campen, L. J. A. M. V., Hoeijmakers, H. W. M., & Mudde, R. F., 2010. Separation of oil droplets in swirling water flow. *7 International Conference on Multiphase Flow*.

[7] Cabral, R. V. & Rocha, A. D., 2017. Projeto do dispositivo gerador de giro de um hidrociclone axial. *X Simpósio de Iniciação Científica da UFABC*.

[8] Fluent, A., 2019. Ansys fluent theory guide.

[9] Roache, P. J., 1994. Perspective: A method for uniform reporting of grid refinement studies. *Journal of Fluids Engineering*, vol. 116, n. 3, pp. 405.